Batteries & Supercaps

Research Article
doi.org/10.1002/batt.202200217

Chemistry Europe
European Chemical Societies Publishing

www.batteries-supercaps.org

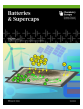

Non-Uniform Distribution of Current in Plane of Large-Area Lithium Electrodes

Saeed Yari,[a, b] Marlies. K. Van Bael,[a, b, c] An Hardy,[a, b, c] and Mohammadhosein Safari*[a, b, c]

This work asserts that increasing the planar area of a lithium (Li) electrode is a challenge in view of ensuring a uniform plating and stripping and spatial uniformity for the state-of-health over the surface of lithium. A significant in-plane heterogeneity is observed for the symmetric Li cells with the stack area in the range of 24 to 96 cm^2. The cycling of the large-area lithium electrodes is performed inside a dedicated home-made electrochemical setup capable of incorporating electrodes of different sizes. The cycling data and post-mortem analysis reveal a clear non-uniformity in the distribution of current and aging for the lithium electrodes having a size larger than the coin-cell and relevant to the commercial applications. It is shown that the inhomogeneous aging manifests mainly in the formation of dead Li film with a spatial variation in thickness and impedance over the surface of the Li electrode.

Introduction

Size is a key design parameter in the development of cost-efficient batteries with high capacity for applications such as electric vehicles and stationary storage. Increasing the thickness of the porous electrodes and the stack area of the cell can provide cost benefits in the manufacturing of lithium-ion batteries by savings in the equipment investment and operational costs related to the coating, calendaring, slitting, and stacking.[1–4] Numerous reports highlight the significant heterogeneity through-plane of the thicker electrodes and its role in the acceleration of aging.[5–11] For instance, the redistribution of carbon-binder domain during the drying step of thicker electrodes is a well-known mechanism that can lend significant through-plane heterogeneity to the electrode microstructure.[12,13] It is, however, very little known about the possible in-plane heterogeneity in large area electrodes and the consequences on performance and longevity of the cell.[14–20] This circumstance can be partly understood for the conventional lithium-ion batteries in view of negligible expected sensitivity of the process-induced heterogeneity to the stack area in contrast to the thickness of the porous electrodes.

In the next generation batteries such as solid-state-lithium and in a broader sense those capitalizing on the metal electrodes such as lithium-sulfur technology, the in-plane heterogeneity over the surface of the electrodes and in particular the lithium (Li) anode deserves special attention due to the peculiar nature of the lithium stripping and plating during cell (dis)charge. Unlike conventional Li-insertion porous electrodes, the morphological details of a planar Li electrode and its complex evolution during cycling (Figure 1a) are decisive to the performance and aging dynamics of the cell.[21–26] Initially a layer of solid electrolyte interphase (SEI) forms on the surface of the lithium. This layer usually lacks sufficient mechanical flexibility and is vulnerable to cracking during the repeated cycling. Upon lithium plating, the SEI layer might crack as the plating is accompanied by the expansion of the electrode (step 1, Figure 1a). This promotes the formation of lithium dendrites at the cracked edges as plating continues (step 2, Figure 1a). During Li stripping, the electrode contraction coupled to the lithium dissolution from the kinks and roots of the dendrites further exacerbates the situation and detaches lithium dendrite from the bulk of the electrode. Therefore, a layer of electronically isolated lithium dendrite accumulates on the electrode surface which is known as "dead lithium" (step 3, Figure 1a). The continuation of this process by further cycling finally results in the conversion of the lithium metal into an expanded porous body which is essentially remnants of the side reactions and a thick layer of dead lithium (step 4, Figure 1a).

In this work, we investigate the inhomogeneity in plane of the planar lithium electrodes and showcase the significant sensitivity of the aging dynamics to the footprint of the lithium electrodes. To do so a series of symmetric Li cells with a large electrode area up to 96 cm^2 are cycled inside a home-made cell enclosure (Figure 1b and c) and the results are discussed with the aid of post-mortem analysis in view of the spatial distribution of the current and state-of-health over the Li electrode's surface. To simply differentiate between the two lithium electrodes in a symmetric cell, we refer to the one undergoing the stripping in the first cycle as positive lithium, and the counter electrode is labelled as negative lithium, in further discussions. A conventional liquid electrolyte is used in the demonstrations to avoid the additional complexities

[a] Dr. S. Yari, Prof. M. K. Van Bael, Prof. A. Hardy, Prof. M. Safari
Institute for Materials Research (IMO-imomec), UHasselt
Martelarenlaan 42, 3500 Hasselt, Belgium
E-mail: momo.safari@uhasselt.be
[b] Dr. S. Yari, Prof. M. K. Van Bael, Prof. A. Hardy, Prof. M. Safari
Energyville
Thor Park 8320, 3600 Genk, Belgium
[c] Prof. M. K. Van Bael, Prof. A. Hardy, Prof. M. Safari
IMEC division IMOMEC
3590, Diepenbeek Belgium

Supporting information for this article is available on the WWW under https://doi.org/10.1002/batt.202200217

Research Article
doi.org/10.1002/batt.202200217
Chemistry Europe
European Chemical Societies Publishing

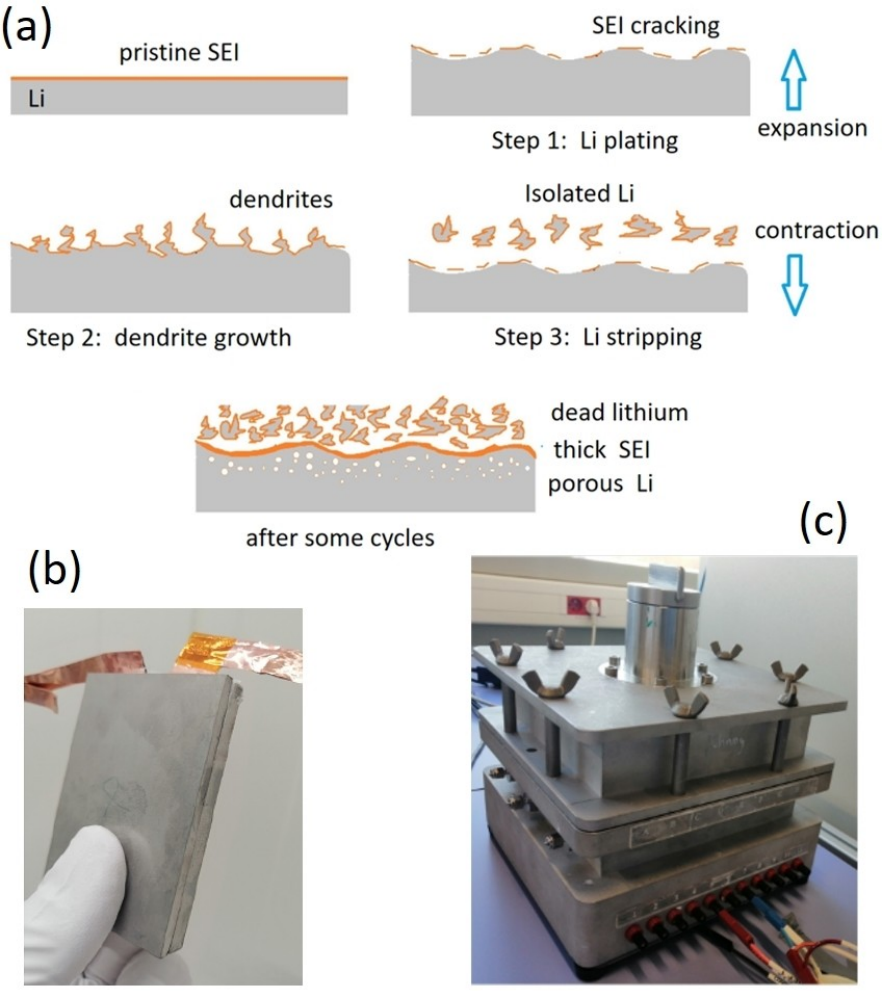

Figure 1. a) A simplified representation of lithium metal degradation during continuous plating and stripping process b) smooth stainless steel plates for pressure application and holding the symmetric lithium stack inside the battery setup, c) home-made battery enclosure setup for battery cycling tests with large area electrodes and with a controlled stack pressure (see SI).

involved with the contact between a solid-electrolyte and lithium.

Results and Discussion

Polarization at large symmetric Li cells

The voltage profile of the large symmetric Li cells during 144 hours of cycling at 0.175 mA/cm^2 is presented for the three distinct electrode sizes of 24, 48, and 96 cm^2 (Figure 2a). The unstable and non-monotonic evolution of voltage is evident whereas the asymmetry between the charge and discharge voltage profiles is rather insignificant (Figure 2b). The positive and negative lithium electrodes at the end of cycling show a clear in-plane heterogeneity with respect to their visual aspects (Figure 2c). In this figure, the locations labelled P1 to P30 identify the samples that were punched out for further image processing and EIS measurement in the coin cells. The voltage profiles reveal a clear rise in the polarization during the first few cycles which can be explained by the formation of SEI layer and the morphological features of the lithium dendrite formed at low currents. The lithium dendrite could take up two general forms known as needle-like or 2D dendrite and mossy-like or 3D dendrites.[23,24,26] It is reported that the 2D dendrites form at the current densities usually below 0.5 mA/cm^2 and are more uniformly distributed and compatible with the growth of SEI layer without causing it to fracture. On the other hand, at higher current densities, the lithium deposits in a more irregular and crooked form and so has a 3D structure. Under constant-current conditions, the initial cycles are associated with the growth of 2D lithium dendrites and formation of a well-preserved SEI layer which explains the gradual increase of polarization and the cell impedance. This situation typically holds for a finite length of time and further continuous cycling turns the 2D structure into a 3D and mossy shape dendrite. The formation of the mossy lithium is associated with a characteristic decay in the cell polarization due to the dramatic increase of the contact area between Li and the electrolyte which is in favour of smaller polarization.[21,24] We should bear in mind that

Research Article
doi.org/10.1002/batt.202200217
Chemistry Europe
European Chemical Societies Publishing

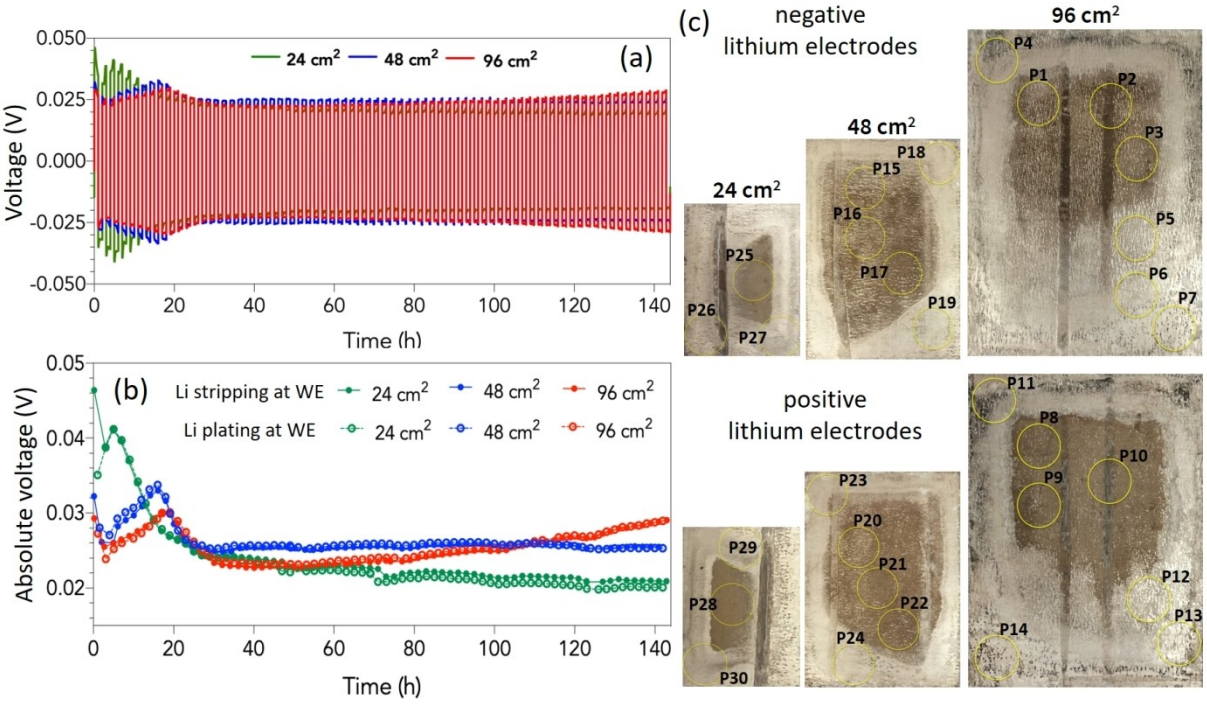

Figure 2. a) voltage-time and b) absolute voltage-time profiles of the symmetric Li-metal batteries during galvanostatic cycling for 144 hours at 0.175 mAh/cm^2, c) optical images of the aged positive and negative lithium electrodes recovered from the cells with different sizes at the end of 144 hours cycling; the location of the small punches, for post-mortem analysis, are indicated by P1–P30.

the growth dynamics of the 2D and 3D lithium and the transition between the two modes is a complex function of the electrolyte composition, current density, cell geometry (coin cell, pouch cell, etc.), and stack pressure among others.[24] As such the observed variation among our samples having different sizes was expected. We specifically observe a higher polarization for the 24 cm^2 electrode during the initial cycles compared to the other two cells (Figure 2a and b). We speculate that the current distribution over the smallest electrode is more uniform and the hot spots are less frequent. This minimizes the probability of having local areas with intensified current densities which can crack the SEI layer and form the mossy and less resistive network of dendrites.

Upon continuous cycling, the 3D growth of lithium becomes the dominant mode, the cell resistance drops, and the cell voltage stabilizes while the dead lithium is accumulating. The thickening of a dead lithium layer is concurrent with the formation of a more tortuous pathway for the transport of lithium ions and gradually increases the impedance of the cells.[22,27,28] After about 30 hours of cycling, the polarization for the three cells levels off around an almost similar value (Figure 2a and b). For the remaining cycles, the cell with 24 cm^2 of area exhibits the least polarization relative to the other two larger cells. The polarization at the electrode with 48 cm^2 of area stays above that of the 96 cm^2 electrode for nearly 100 hours of cycling. Noteworthy is the instability of the largest cell compared to the smaller cells. Although the polarization of the cells with 24 and 48 cm^2 area reaches an approximate steady state after ~30 hours, the voltage profile of 96 cm^2 cell only remains stable between 30 to 60 hours. After 60 hours, a continuous and steep rise in the polarization of the largest cell bespeaks a more complicated dynamics of resistance build up compared to the smaller lithium cells.

Spatial non-uniformity

The individual punches (P1–P30) were analysed to obtain more information from different locations on the surface of the electrodes at the end of cycling. Two distinct dark and bright zones over the surface of the aged electrodes are discernible. The EIS response of individual punches from both regions were measured in a coin cell in front of a pristine Li as counter electrode and using a fresh electrolyte and separator. Prior to the EIS measurements, the surface of the pristine lithium was conditioned for one cycle at $\pm$0.0175 mA/cm^2 for 2 hours. The EIS was also measured for a fresh (and conditioned) symmetric Li coin-cell in order to subtract the contribution of the pristine Li electrode from the overall impedance of the coin cells assembled with the aged and pristine lithium. By doing so, we could approximate the distribution of the impedance over the surface of the large Li electrodes (Figure 3). Although the largest and lowest impedance values were recorded for the samples from the dark and bright regions, respectively, but no direct correlation can be detected between the impedance values and the location on the electrode (see SI). The wide range of the impedance values however suggests that the current distribution over the surface of large lithium electrodes is very non-uniform. One can allocate 10%, 23.3%, 46.6%, 13%, 3.3% and 3.3% of the P1–P30 samples to the impedance

Research Article
doi.org/10.1002/batt.202200217
Chemistry Europe
European Chemical Societies Publishing

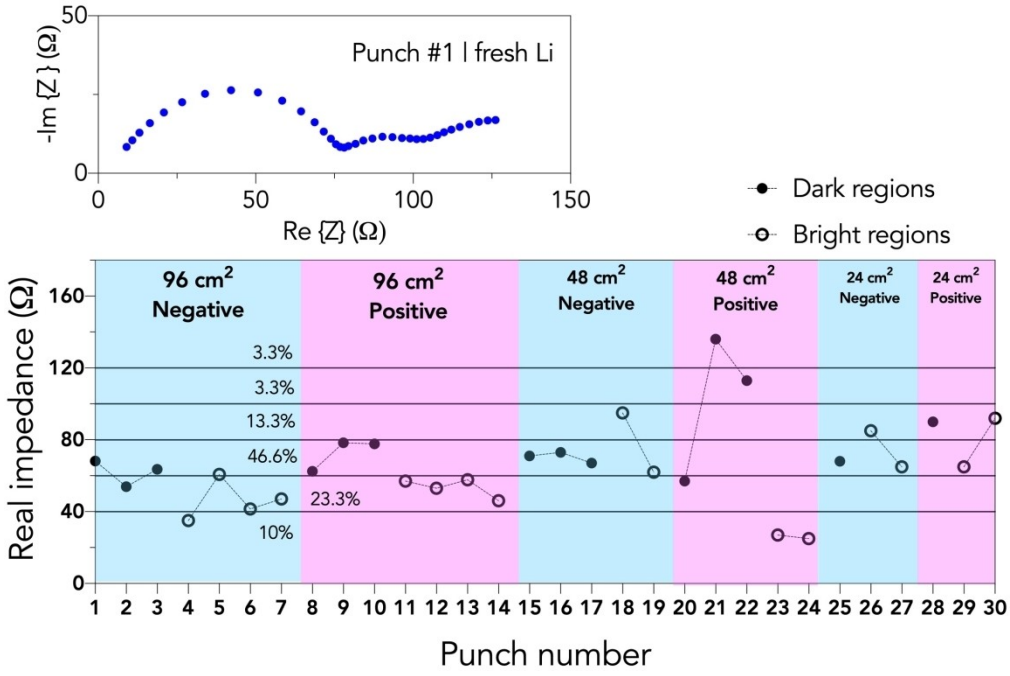

Figure 3. EIS of individual punches taken from the larger electrodes. The values correspond to the real impedance of the large semi-circle in the Nyquist plot. The percentage of impedance distribution in selected ranges is also reported.

ranges of 0–40 Ω, 40–60 Ω, 60–80 Ω, 80–100 Ω, 100–120 Ω, and above 120 Ω, respectively. This observation shows that each sample has experienced a different load profile history in the larger electrodes depending on the sample location and size of the cell. Figure 4 shows the optical images of the lithium electrodes cycled in a series of coin cells at ±0.044, ±0.175, ±0.35, ±0.525, and ±0.7 mA/cm^2 from top (Figure 4a) and side (Figure 4b) views. A dead Li layer is growing at the lithium electrodes and turns the electrodes darker. The darkness of the electrodes appears to be proportional to the thickness of the dead Li layer (Figure 4a and b). The growth of dead lithium layer results in the expansion of the electrode to a thickness

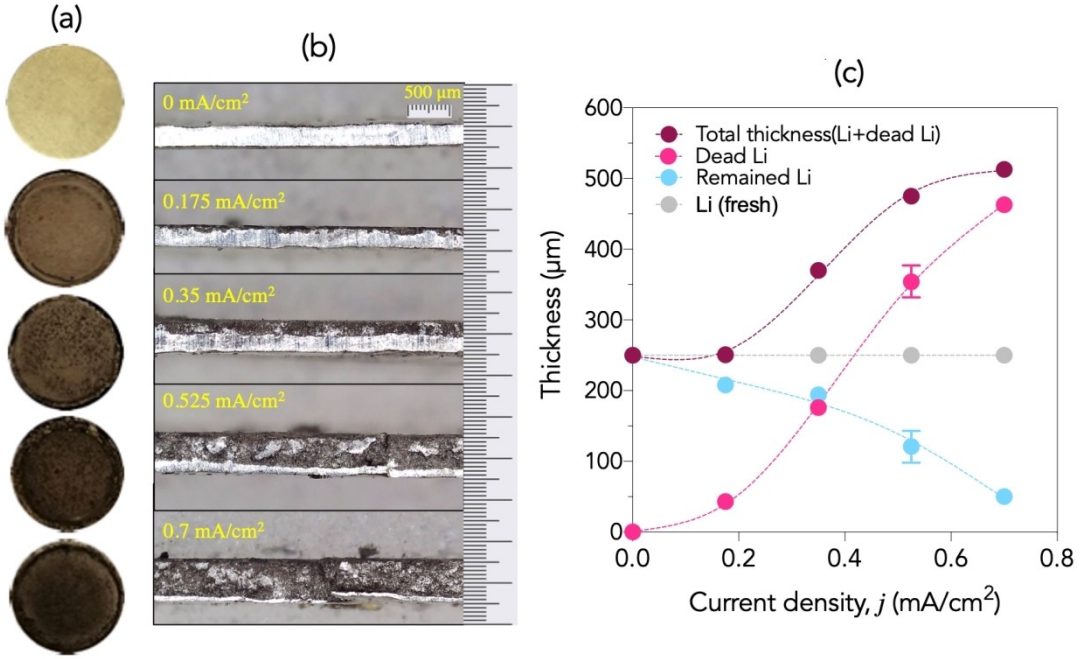

Figure 4. Lithium electrodes recovered from the symmetric Li coin cells cycled at different current densities for 144 hours a) surface images, b) cross-sectional images, c) thickness variation of the dead lithium, remained lithium, and total electrode thickness as function of current density.

twice the thickness of the pristine electrode for the coin cell cycled at 0.7 mA/cm^2 (Figure 4c).

The thickness of the residual Li has a lower sensitivity to the current density at lower currents, but if the current density exceeds 0.35 mA/cm^2, Li deteriorates at a higher rate. Similarly, the formation of dead Li accelerates by increasing the current density. One explanation for the higher rate of degradation at higher current densities is the faster pile-up of dead Li which exacerbates diffusion of Li ions through the tortuous dead Li layer resulting in a higher polarization that further accelerates degradation. An estimation for the current distribution over the surface of large area electrodes might be obtained by assuming that the local thickness of lithium is directly correlated with the degree of aging and indirectly with the local current density. Similar to the impedance data, the thickness of P1 to P30 samples (Figure 5) are distributed over a wide range with a clearly higher thickness in the darker zones of the electrodes. The minimum total thickness value (lithium + dead lithium) is at 125 μm which corresponds to a fresh lithium and the maximum of 260 μm was recorded for P9 at 96 cm^2 positive electrode. We should note that our statement of a darker region having a thicker dead lithium layer, is to a great extent representative of the trend that we observed in most samples, though it bears some uncertainty. For example, the error bars in Figure 5 (and specifically for the dark regions) are quite large, and that is because even in a single electrode punch there were very big differences in thickness depending on the exact location of the measurement probe (the tip of the micrometer was about 3 mm). However, such a large variation in the thickness of aged lithium electrodes strengthens the hypothesis of very non-uniform current distribution in-plane of our electrodes. The grey-level image histograms of the lithium electrodes aged in the coin cells at different current densities together with the histograms of the large-area electrodes were analysed to quantify the correlation between the local aging status and the current distribution. Every pixel in the digital images is characterized by a grey level value (i) between 0 to 255, where 0 represents the darkest and 255 the brightest level. An image histogram shows the distribution of these grey-level intensities by counting the number of pixels at each intensity. Based on the image histogram, we can estimate the fraction of area that corresponds to each grey-level value (i) by Equation (1):

$$A^i = \frac{\mathrm{cn}^i}{\mathrm{cn}^t} \tag{1}$$

where cn^i is the pixel count at the grey-level i and cn^t is the sum of pixel counts at all grey-level values. The normalized image histograms for the lithium electrodes aged at different current densities, in the coin cells, demonstrate certain characteristic peaks (Figure 6a). The presence of sharp peaks in Figure 6a suggests that the surface features in the coin cells are rather homogenous. At very high current densities, however, the peaks are wider and less sharp that points out to some degree of inhomogeneity even in the coin cells. We can use these characteristic peaks to set up an approximate correspondence between the grey-level values and the current density. Prior to this, we need to find the domain's probability density function, because there are overlaps among the peaks [Equation (2)]:

$$P_j^i = \frac{A_j^i}{\sum_{j=1}^{6} A_j^i} \tag{2}$$

where P_j^i (Figure 6b) is the probability at which an area with a grey-level i might be associated with the degradation contributed from the different levels of current density (j). Here, A_j^i is the fractional area based on the histograms of lithium from the coin-cells (Figure 6a). We can further approximate the fractional area of a large area Li electrode (S_j) which is subject to the local current density level of j [see Equation (3)]:

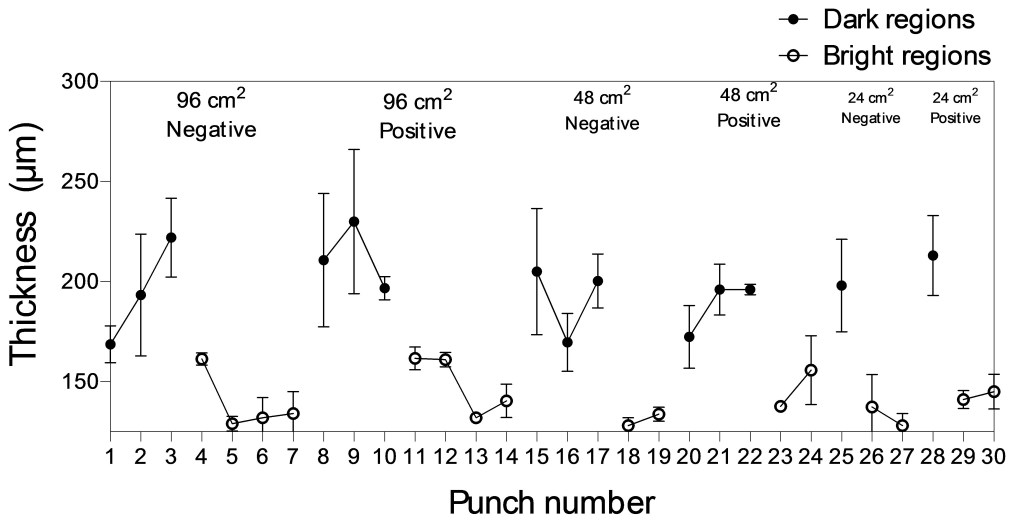

Figure 5. Thickness profile for individual punches taken from the degraded large Li electrodes. The initial lithium thickness was 125 μm.

Research Article
doi.org/10.1002/batt.202200217
Chemistry Europe
European Chemical Societies Publishing

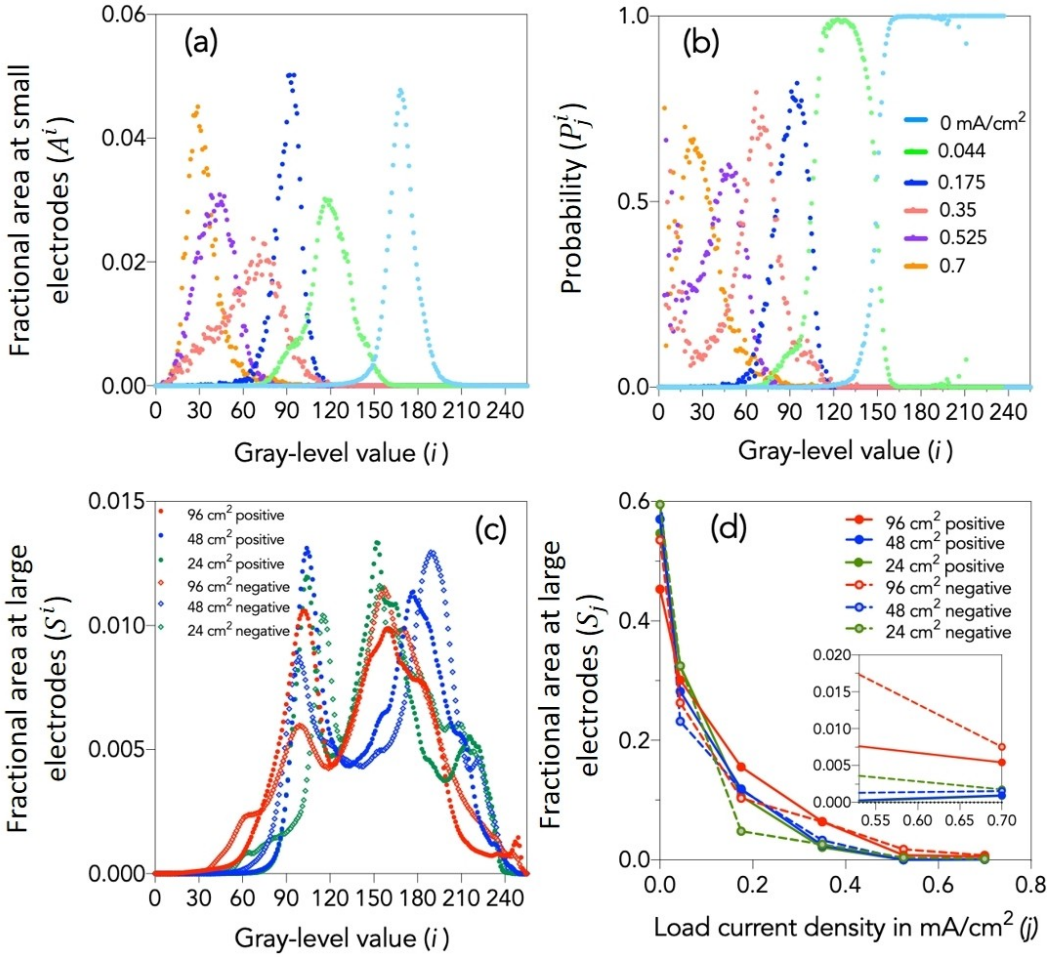

Figure 6. a) The normalized image histograms for small-format cycled electrodes (see Figure 4a) that correlates the fractional area corresponding to a gray level to a known current density. The darkest pixels are at the left (min = 0) and the one for brightest pixels are at the right (max = 255), b) probability density distribution of a certain gray-level value being related to degradation at a known current density, c) gray-level value histogram for large format degraded electrodes, d) fraction of the area on the degraded large-format Li metal electrodes that corresponds to degradation at certain current density.

$$S_j = \sum_{i=0}^{255} S^i P_j^i \tag{3}$$

where S^i corresponds to the fractional area of a large lithium electrode with a grey-level of i that is available from the histograms of Figure 6(c).

The non-uniform degradation at large electrodes is manifested in the wide distribution of grey-level values and the presence of multiple peaks compared to the histogram of the lithium electrodes from the coin cells (Figure 6b). The non-uniform distribution of the current over the surface of large electrodes is demonstrated in Figure 6d using the estimated current histogram [S_j from Equation (3)].

Conclusion

An experimental approach was used to showcase how enlarging the planar surface of lithium electrodes can amplify the effects of non-uniform distribution of current and aging which are invisible and usually overlooked when working with the small coin cells. The stack area of a cell with lithium electrode is shown to be an important parameter to be investigated further for the optimization of the next generation batteries with lithium anode.

Lithium metal electrodes with 24, 48 and 96 cm^2 surface area were cycled in a dedicated setup and with a symmetric Li | Li configuration and liquid electrolyte. The voltage-time profiles for all large format cells during cycling at 0.175 mAh/cm^2 showed an initial rise which is characteristic of 2D and needle shape lithium dendrite growth. The initial increase in the polarization was higher for the smaller (24 cm^2) electrode, which was related to a more uniform distribution of the current over the surface of the electrode and a growth of the SEI layer without significant cracking. The cell polarization stabilized after 30 hours of cycling for the 24 and 48 cm^2 area electrodes while the 96 cm^2 cell exhibited a steady rise in the polarization after 60 hours of cycling. In the post-mortem analysis, the EIS and simple image processing of the recovered electrodes sampled at different locations over the surface were used to investigate the heterogeneity in-plane of the electrodes. The Li electrodes demonstrated a large spatial variance for the thick-

ness of the dead lithium and the impedance pointing out to a very non-uniform distribution of the current and aging.

The simple methodology followed in this work provided semi-quantitative information about the significance of the in-plane heterogeneity in the large area lithium electrodes with conventional liquid electrolytes. A similar approach can be used to conduct a systematic investigation of the effect of size and geometry for the lithium electrodes for the next generation technologies like solid-state lithium, while considering extra parameters such as the stack pressure and temperature.

Experimental

Large format Li metal electrodes were manually prepared by roll pressing a thin foil of lithium (125 μm) on a copper current collector. Electrodes were in three different sizes of 24 cm^2, 48 cm^2 and 96 cm^2 with identical shape format. The aspect ratio of the electrodes (length/width ratio) was similar at 1.33, the width of the current collecting tab was 0.22 that of the electrode width, and the shortest distance from the centre of the tab to the electrode edges was set at 0.25 times the width of the electrode (see SI).

Symmetric Li cells were assembled inside an argon filled glovebox (H_2O and $O_2 < 1$ ppm). The two Li electrodes were placed in between two flat and rigid stainless steel plates as the holder and casing of the electrodes to ensure a uniform distribution of pressure over the surface of the electrodes (Figure 1b). The Whatman GF/C borosilicate glass microfiber filter was used as the separator with 260 μm thickness and approximately 90% porosity. Though the glass fiber filter is slightly thick, it provides a sufficiently high degree of electrolyte wetting with 50 μL/cm^2 of EC:EMC (3:7), 1 M $LiPF_6$ electrolyte. The higher thickness is also necessary to ensure a high mechanical stability and sufficient retention of electrolyte for our model experimental system. The cell stack was placed inside a home-made larger set-up which was designed to provide an air-tight environment, with specific wirings and electrical feedthrough to bring the current in and out of the battery cell. A spring driven plate inside the set-up was used to apply 2 N/cm^2 of pressure on the electrode stack (Figure 1c, see Supporting Information). Based on our observations, this was a pressure good enough to provide a good contact among the cell components. Further work, however, is required to investigate the possible sensitivity of the in-plane heterogeneity to the stack pressure.

Biologic VMP3 potentiostat (±10 V) was used to cycle the cells for a duration of 144 hours with an applied constant-current density of ±0.175 mA/cm^2 (equivalent to C/10 in a typical Li-ion battery with the NMC loading of 10 mg/cm^2 at the cathode). Next to the large cells, a series of symmetric Li coin cells (~1.76 cm^2) were prepared and cycled for the same duration (144 hours) at different current densities ±0.044, ±0.175, ±0.35, ±0.525, and ±0.7 mA/cm^2. At the end of cycling, all the cells were disassembled inside a dry room (dew point −45 °C) and the electrodes were recovered for post-mortem analysis. In the case of larger cells, a total of 30 small punches from different regions were cut out from the positive and negative electrodes for further analysis, labelled as P1 to P30. Images were captured from the samples and processed with the open source ImageJ software. Cross sectional images from the aged lithium electrodes were obtained by digital microscope in the dry room environment to quantify the thickness of lithium and dead lithium layer by holding the sample between two glass plates of which the side was exposed parallel to the direction of microscope's light. The electrochemical impedance spectroscopy (EIS) response of the aged samples were measured in a frequency range of 10 mHz to 10 kHz and with an excitation amplitude of 5 mV in a coin cell using a fresh electrolyte and separator and a pristine Li counter electrode.

Supporting Information

Supporting Information is available from the Wiley Online Library or from the author.

Acknowledgements

The authors are grateful for financial support to the Special Research Fund BOF of Hasselt University. S. Y. and M.S. acknowledge Johnny Baccus and Jan Mertens for the technical support.

Conflict of Interest

The authors declare no conflict of interest.

Data Availability Statement

The data that support the findings of this study are available from the corresponding author upon reasonable request.

Keywords: dead lithium · lithium-metal electrode · large area electrodes · non-uniform

[1] F. Duffner, L. Mauler, M. Wentker, J. Leker, M. Winter, *Int. J. Prod. Econ.* **2021**, *232*, 107982.
[2] D. L. Wood, J. Li, C. Daniel, *J. Power Sources* **2015**, *275*, 234–242.
[3] A. Sakti, J. J. Michalek, E. R. H. Fuchs, J. F. Whitacre, *J. Power Sources* **2015**, *273*, 966–980.
[4] R. E. Ciez, J. F. Whitacre, *J. Power Sources* **2017**, *340*, 273–281.
[5] T. Sasaki, C. Villevieille, Y. Takeuchi, P. Novak, *Adv. Sci.* **2015**, *2*, 1500083.
[6] F. M. Kindermann, P. J. Osswald, G. Ehlert, J. Schuster, A. Rheinfeld, A. Jossen, *J. Electrochem. Soc.* **2017**, *164*, E3105-E3113.
[7] N. Ghanbari, T. Waldmann, M. Kasper, P. Axmann, M. Wohlfahrt-Mehrens, *J. Phys. Chem. C* **2016**, *120*, 22225–22234.
[8] H. Zhou, K. An, S. Allu, S. Pannala, J. Li, H. Z. Bilheux, S. K. Martha, J. Nanda, *ACS Energy Lett.* **2016**, *1*, 981–986.
[9] S. Yari, H. Hamed, J. D'Haen, M. K. Van Bael, F. Uwe Renner, A. Hardy, M. Safari, *ACS Appl. Energ. Mater.* **2020**, *3*, 11820–11829.
[10] H. Hamed, S. Yari, J. D'Haen, F. Uwe Renner, N. Reddy, A. Hardy, M. Safari, *Adv. Energy Mater.* **2020**, 10, 2002492.
[11] Y. Yang, R. Xu, K. Zhang, S.-Jun Lee, Li. Mu, P. Liu, C. K. Waters, S. Spence, Z. Xu, C. Wei, D. J. Kautz, Q. Yuan, Y. Dong, Y.-Sang Yu, X. Xiao, H.-Koo Lee, P. Pianetta, P. Cloetens, J.-Sik Lee, K. Zhao, F. Lin, Y. Liu, *Adv. Energy Mater.* **2019**, *9*, 1900674.
[12] L. S. Kremer, A. Hoffmann, T. Danner, S. Hein, B. Prifling, D. Westhoff, C. Dreer, A. Latz, V. Schmidt, M. Wohlfahrt-Mehrens, *Energy Technol.* **2019**, *8*, 1900167.
[13] S. Jaiser, M. Müller, M. Baunach, W. Bauer, P. Scharfer, W. Schabel, *J. Power Sources* **2016**, *318*, 210–219.
[14] M. Katayama, K. Sumiwaka, R. Miyahara, H. Yamashige, Y. Hisao, A. Hajime, U. Yoshiharu, O. Toshiaki, I. Yasuhiro, Z. Ogumi, *J. Power Sources* **2014**, *269*, 994–999.
[15] X. Yu, Z. Feng, Y. Ren, D. Henn, Z. Wu, K. An, B. Wu, C. Fau, C. Li, S. J. Harris, *J. Electrochem. Soc.* **2018**, *165*, A1578-A1585.

[16] P. Taheri, A. Mansouri, B. Schweitzer, M. Yazdanpour, M. Bahrami, *J. Electrochem. Soc.* **2013**, *160*, A1731-A1740.
[17] W. A. Paxton, Z. Zhong, T. Tsakalakos, *J. Power Sources* **2015**, *275*, 429–434.
[18] G.-H. Kim, K. Smith, K.-J. Lee, S. Santhanagopalan, A. Pesaran, *J. Electrochem. Soc.* **2011**, *158*, A955.
[19] G. Zhang, L. Cao, S. Ge, C.-Y. Wang, C. E. Shaffer, C. D. Rahn, *J. Electrochem. Soc.* **2014**, *161*, A1499-A1507.
[20] J. B. Robinson, J. A. Darr, D. S. Eastwood, G. Hinds, P. D. Lee, P. R. Shearing, O. O. Taiwo, D. J. L. Brett, *J. Power Sources* **2014**, *252*, 51–57.
[21] G. Bieker, M. Winter, P. Bieker, *Phys. Chem. Chem. Phys.* **2015**, 17, 8670.
[22] K.-Hung Chen, K. N. Wood, E. Kazyak, W. S. LePage, A. L. Davis, A. J. Sanchez, N. P. Dasgupta, *J. Mater. Chem. A* **2017**, 5, 11671–11681.
[23] JuHsiang Cheng, A. A. Assegie, C.-Jui Huang, M.-Hsien Lin, A. M. Tripathi, C.-Chieh Wang, M. T. Tang, Y.-Fang Song, W.-Nien Su, B. J. Hwang, *J. Phys. Chem. C* **2017**, *121*, 7761–7766.
[24] K. N. Wood, M. Noked, N. P. Dasgupta, *ACS Energy Lett.* **2017**, *2*, 664–672.
[25] D. Lin, Y. Liu, Y. Cui, *Nat. Nanotechnol.* **2017**, *12*, 194–206.
[26] J. Steiger, D. Kramer, R. Mönig, *J. Power Sources* **2014**, *261*, 112–119.
[27] S. Xu, K.-H. Chen, N. P. Dasgupta, J. B. Siegel, A. G. Stefanopoulou, *J. Electrochem. Soc.* **2019**, *166*, A3456-A3463.
[28] M. Nagasaki, K. Nishikawa, K. Kanamura, *J. Electrochem. Soc.* **2019**, *166*, A2618-A2628, 2019.

Manuscript received: May 12, 2022
Revised manuscript received: June 29, 2022
Version of record online: July 14, 2022